Detection of Architectural Distortion in Prior Mammograms Using Statistical Measures of Orientation of Texture

Jayasree Chakraborty[a], Rangaraj M. Rangayyan[b,c,⋆], Shantanu Banik[b], Sudipta Mukhopadhyay[a], and J. E. Leo Desautels[b]

[a]Department of Electronics and Electrical Communication Engineering
Indian Institute of Technology Kharagpur, West Bengal, India 721 302
[b]Department of Electrical and Computer Engineering, Schulich School of Engineering
[c]Department of Radiology, University of Calgary, Calgary, Alberta, Canada T2N 1N4

ABSTRACT

We present a method using statistical measures of the orientation of texture to characterize and detect architectural distortion in prior mammograms of interval-cancer cases. Based on the orientation field, obtained by the application of a bank of Gabor filters to mammographic images, two types of co-occurrence matrices were derived to estimate the joint occurrence of the angles of oriented structures. For each of the matrices, Haralick's 14 texture features were computed. From a total of 106 prior mammograms of 56 interval-cancer cases and 52 mammograms of 13 normal cases, 4,224 regions of interest (ROIs) were automatically obtained by applying Gabor filters and phase portrait analysis. For each ROI, statistical features were computed using the angle co-occurrence matrices. The performance of the features in the detection of architectural distortion was analyzed and compared with that of Haralick's features computed using the gray-level co-occurrence matrices of the ROIs. Using logistic regression for feature selection, an artificial neural network for classification, and the leave-one-image-out approach for cross-validation, the best result achieved was 0.77 in terms of the area under the receiver operating characteristic (ROC) curve. Analysis of the free-response ROC curve yielded a sensitivity of 80% at 5.4 false positives per image.

Keywords: Architectural distortion, angle co-occurrence matrix, breast cancer, computer-aided diagnosis, feature extraction, Haralick's texture features, mammography, prior mammograms.

1. INTRODUCTION

Architectural distortion is the third most common finding of nonpalpable breast cancer in mammographic images.[1] This sign of cancer comprises distortion of the normal architecture of the breast with no definite mass visible; the associated patterns include spiculations radiating from a point or focal retraction at the edge of the breast parenchyma.[2] Due to its subtle nature and variability in appearance, architectural distortion is often missed in mammographic screening for breast cancer.[1] Various computer-aided diagnosis (CAD) systems and effective techniques are available to detect the commonly observed signs of breast cancer, such as masses and calcifications,[3,4] but efficient techniques for the detection of architectural distortion are not yet available.[5,6]

Karssemeijer and te Brake[7] proposed a multiscale-based method for the detection of stellate patterns related to masses and architectural distortion, and achieved a sensitivity of about 90% at one false positive (FP) per image with 50 mammographic images from the MIAS database.[8] Ayres and Rangayyan[9] proposed a method based on Gabor filters and phase portraits to detect architectural distortion. Rates of sensitivity of 84% at 4.5 FP/image and 81% at 10 FP/image were obtained with two different datasets. Jasionowska et al.[10] applied Gabor filters and the two-dimensional Fourier transform in polar coordinates to detect architectural distortion.

The techniques mentioned above were applied to mammograms on which cancer was detected by radiologists (known as diagnostic or detection mammograms). However, for the detection of breast cancer, simultaneous analysis of the current and prior mammograms is often recommended.[11,12] It has been observed that prior mammograms (images obtained in a screening program before the detection of breast cancer) could often provide

⋆ To whom all correspondence should be addressed: ranga@ucalgary.ca

Medical Imaging 2012: Computer-Aided Diagnosis, edited by Bram van Ginneken, Carol L. Novak,
Proc. of SPIE Vol. 8315, 831521 · © 2012 SPIE · CCC code: 1605-7422/12/$18 · doi: 10.1117/12.910937

information that could assist in the detection of subtle signs of abnormalities in cases of screen-detected[13] or interval cancer.[14–17] Only a few studies have been reported on the analysis of prior mammograms. Banik et al.[16] proposed methods based on Gabor filters, phase portraits, fractal dimension, and angular spreads of power, Gabor magnitude response, Gabor filter angle, coherence, and orientation strength.[17,18] A sensitivity of 80% with 5.8 FP/image was achieved with a dataset of 106 prior and 52 normal mammographic images.[16]

The aim of the present study is to develop a CAD technique for the detection of architectural distortion in prior mammograms of interval-cancer cases with high sensitivity and low FP rates. A bank of Gabor filters and phase portrait analysis were used for the detection of suspicious regions with architectural distortion.[17,18] The main contribution of the present work is the derivation of statistical features based on the co-occurrence matrices of the angle of oriented patterns in the suspicious regions. The features are shown to provide good discrimination between FP regions and true-positive (TP) regions, and assist in the detection of architectural distortion.

2. MATERIALS AND METHODS

2.1 Detection of potential sites of architectural distortion

The procedure for the detection of potential or suspicious sites of architectural distortion includes the following steps:[16] segmentation of the breast region using Otsu's thresholding method, extraction of the orientation field using Gabor filters, selection of curvilinear structures, filtering and down-sampling of the orientation field, modeling of phase portraits, and detection of potential sites of architectural distortion. The node map obtained from phase portrait analysis is used to detect peaks related to potential sites of architectural distortion. The results of these steps are illustrated in Figures 1 and 2. However, the procedure results in a number of FP sites that need to be eliminated by further processing.

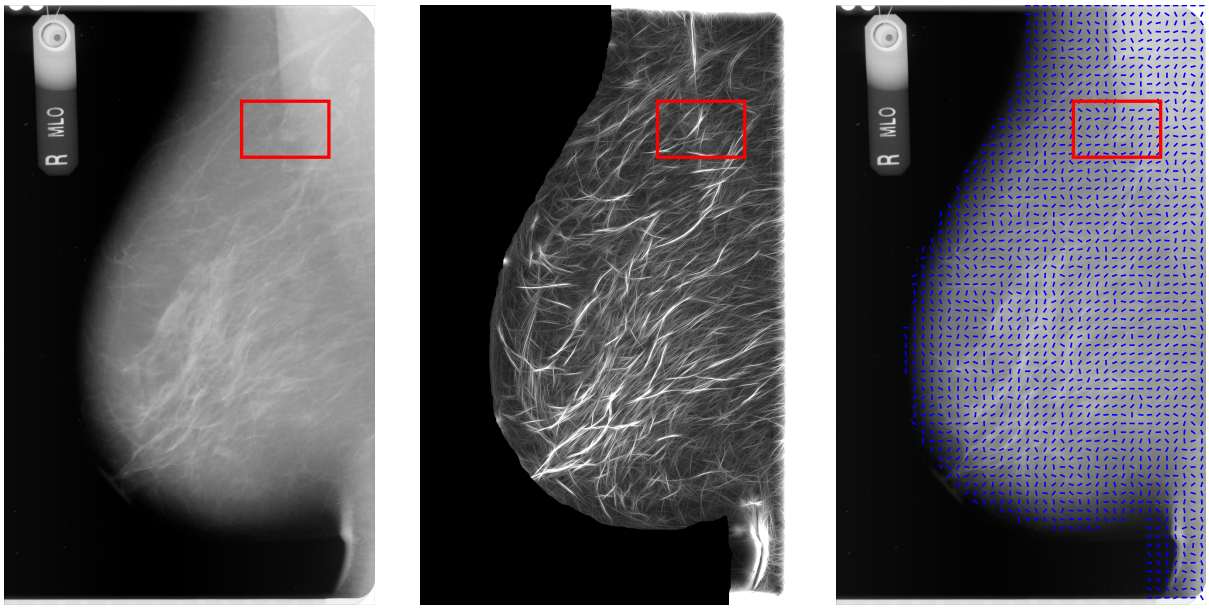

(a) (b) (c)

Figure 1. (a) The prior mammogram of an interval-cancer case. The rectangular box (40.1 mm×25.7 mm) represents the area of architectural distortion drawn by the radiologist. (b) Magnitude response obtained by using 180 real Gabor filters. (c) Orientation field angle superimposed on the mammogram; needles are drawn for every 20^{th} pixel.

2.2 Experimental setup

Experiments were conducted on 158 mammographic images obtained from Screen Test: Alberta Program for the Early Detection of Breast Cancer.[19,20] The dataset contains 106 prior mammographic images of 56 interval-cancer cases and 52 images of 13 normal cases. The images were digitized at 50 μm/pixel and 12 bits/pixel, but

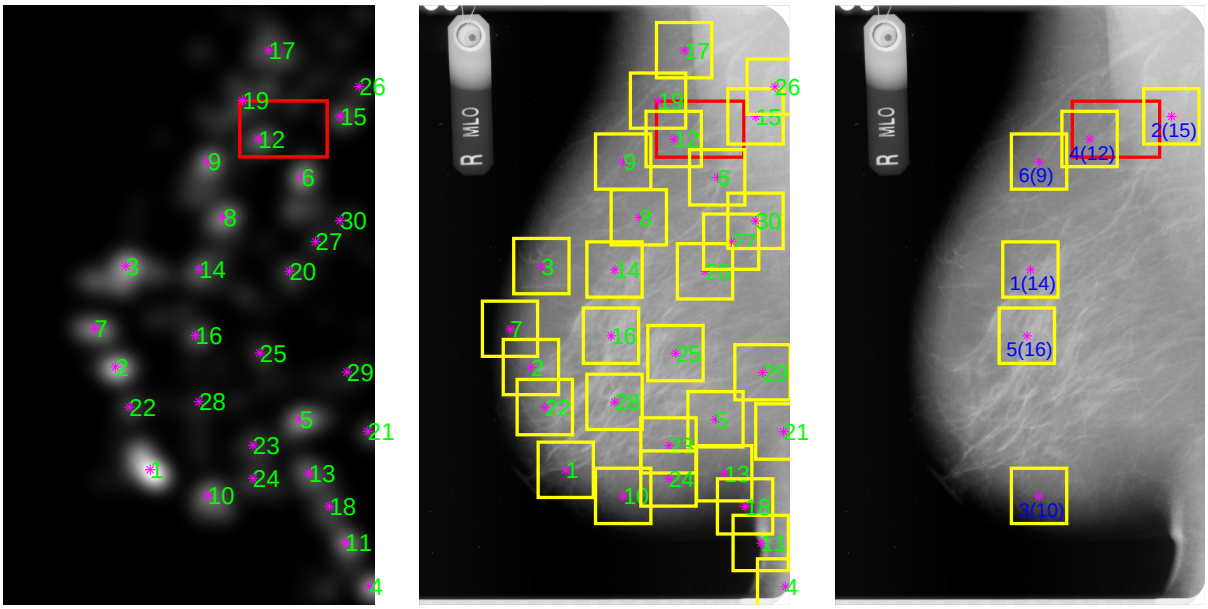

(a) (b) (b)

Figure 2. (a) The node map for the mammogram shown in Figure 1. Asterisk marks (*) represent the peak positions detected automatically in the node map. The numbers next to the asterisks correspond to the peaks in descending order of magnitude. (b) The 30 ROIs, each of size 128×128-pixel (except at the edges), obtained by using the peaks detected in the node map. (c) ROIs after FP reduction by using the ANN classifier and selected features with the leave-one-image-out method. Only the top six ROIs are shown in the image at the associated sensitivity of 80% obtained with 5.5 FP/image. The numbers outside the parentheses correspond to the ranking based on the discriminant values obtained by the ANN classifier and the numbers within the parentheses represent the earlier ranking based on the node value obtained by the method described in Section 2.1.

filtered and down-sampled to 200 μm/pixel and 8 bits/pixel for processing with Gabor filters. The interval-cancer cases used in the present study were acquired in the last scheduled visit to the screening program prior to the detection of cancer. The detection mammograms were not available for this study. A radiologist specialized in screening mammography (J.E.L.D.) evaluated independently the 106 prior mammograms of interval-cancer cases and marked the suspicious regions with architectural distortion using rectangular boxes based on the reports available on subsequent imaging or biopsy, or by detailed inspection of the mammograms.

A total of 4,224 ROIs, including 2,821 ROIs from the interval-cancer cases with 301 ROIs related to the sites of architectural distortion and 1,403 ROIs from the normal cases, of size 128×128 pixels at 200 μm/pixel (except at the edges of the images), were automatically obtained by the method described in Section 2.1. Based on the decreasing order of the peak values in the node maps, up to 30 ROIs were selected per mammogram with their centers at the locations indicated by the peaks. The ROIs having their centers within the areas of architectural distortion marked by the radiologist were labeled as TP ROIs and the others were labeled as FP ROIs. Phase portrait analysis (at 800 μm/pixel) could not detect any TP ROI in one prior mammogram.

2.3 Feature extraction

Normal tissues in the breast parenchyma typically converge toward the nipple; however, the direction of convergence could be changed locally in the presence of architectural distortion. Therefore, analysis of orientated patterns, obtained by the application of a bank of Gabor filters on the mammographic images, could assist in the characterization of the sites of architectural distortion. Figures 3 and 4 show a TP ROI and an FP ROI with their corresponding Gabor magnitude and orientation field responses. It is evident that the TP ROI includes more intersecting tissue structures spread over a wider angular range than the FP ROI.

In the present study, the oriented patterns in the automatically detected suspicious regions were statistically analyzed by using Haralick's 14 texture features.[21,22] In most works on the analysis of texture, Haralick's features are computed based upon the moments of probability density functions (PDFs) estimated using gray-level co-occurrence matrices (GCMs). On the contrary, in the present study, two types of co-occurrence matrices were developed to characterize the nature of oriented patterns based on the co-occurrence of the angles in the orientation fields obtained using Gabor filters, which are referred to as angle co-occurrence matrices (ACMs). The matrix $\mathrm{ACM}_{(l,\theta)}(i,j)$ represents the probability of occurrence of the pair of angles (i,j) at two pixels separated by a distance of l and an angle of θ. The first ACM was computed using only the orientation field angle information and normalized as

$$\mathrm{ACM1}_{(l,\theta)}(i,j) = \frac{P_a(i,j)}{\sum_{i=1}^{N_\theta}\sum_{j=1}^{N_\theta} P_a(i,j)},$$

where $P_a(i,j)$ represents the number of co-occurrences of a pixel with the orientation field angle i and another pixel with the angle j with the separation between the pixels specified by (l,θ), and N_θ is the quantized number of angles (in the present work, $N_\theta = 64$). The second ACM was computed in a similar manner but the associated Gabor magnitude responses were used to increment the elements of the co-occurrence matrix and normalized as

$$\mathrm{ACM2}_{(l,\theta)}(i,j) = \frac{P_m(i,j)}{\sum_{i=1}^{N_\theta}\sum_{j=1}^{N_\theta} P_m(i,j)},$$

where $P_m(i,j)$ is the sum of the Gabor magnitude responses of all of the pixel pairs having angles i and j, with separation by distance l and angle θ.

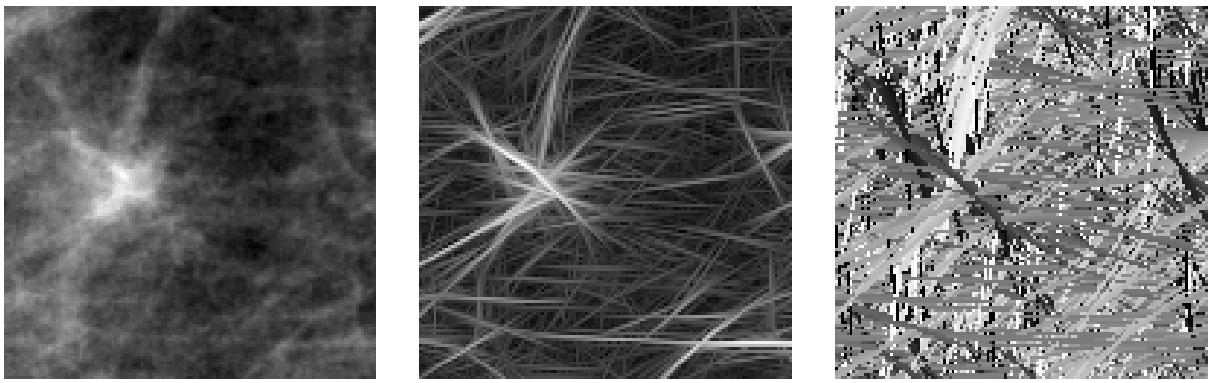

(a) (b) (c)

Figure 3. (a) A 128×128-pixel TP mammographic ROI with architectural distortion. (b) Gabor magnitude response. (c) Orientation field displayed by converting the angle data to gray levels in the range [0, 255].

For each ROI and each type of ACM, four normalized ACMs were calculated with unit pixel distance (l) and angles $\theta = 0\,^\circ, 45\,^\circ, 90\,^\circ$, and $135\,^\circ$. The four ACMs were then averaged to form a single matrix for each ROI for the computation of Haralick's features.

2.4 Feature selection and pattern classification

From the two co-occurrence matrices, two sets of Haralick's 14 features (referred to as H_1 and H_2) were computed to characterize each ROI. For comparative analysis, Haralick's features with the GCM (H_0) were also computed for each ROI. Stepwise logistic regression was applied to each set for feature selection. Fisher linear discriminant analysis (FLDA),[23] the Bayesian classifier,[23] and an artificial neural network (ANN) classifier[24] with one hidden layer containing one neuron and a logistic activation function were used for classification of the ROIs. The leave-one-image-out method was included in the procedures for feature selection and pattern classification. Analysis using the leave-one-patient-out method for feature selection and pattern classification was also performed.

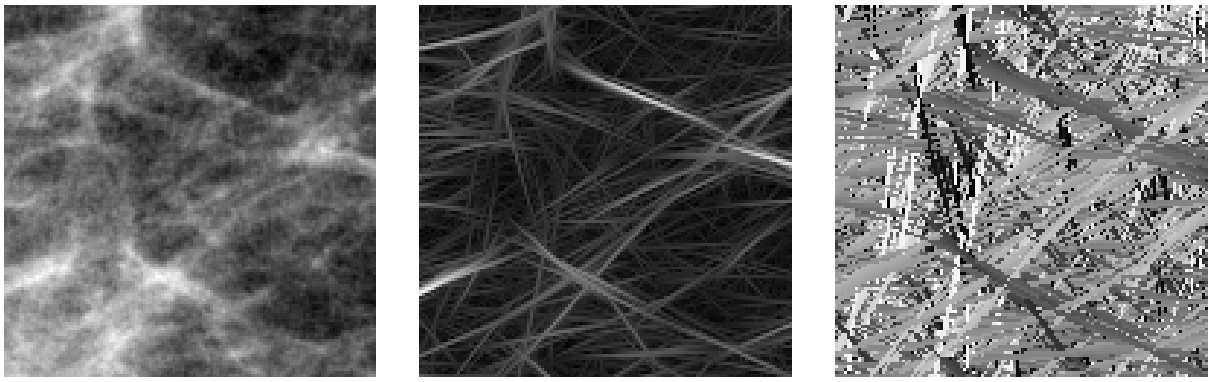

(a) (b) (c)

Figure 4. (a) A 128×128-pixel FP mammographic ROI. (b) Gabor magnitude response. (c) Orientation field displayed by converting the angle data to gray levels in the range [0, 255].

3. RESULTS AND DISCUSSION

The classification performance of the three feature sets derived in the present work with the leave-one-image-out and the leave-one-patient-out methods are listed in Tables 1 and 2, respectively, in terms of the area (A_z) under the receiver operating characteristic curve (ROC) as well as the sensitivity and FP rates obtained by free-response ROC (FROC) analysis. With the leave-one-image-out method, the best performance with A_z = 0.77 was achieved using the ANN and the H_1 feature set. FROC analysis indicated a sensitivity of 80% at 5.5 FP/image with the ANN classifier for H_1, and a sensitivity of 80% at 5.4 FP/image with FLDA for H_2. In most of the cases, H_1 provided better results than H_2 with the leave-one-image-out method. The reduction of FPs by applying the H_1 feature set and the ANN classifier is demonstrated in Figure 2(c) for the mammogram shown in Figures 1 and 2. Based on the discriminant values, only the top six ROIs are shown, with the associated sensitivity of 80% at 5.5 FP/image.

Table 1. Results of ROC and FROC analysis by using selected features based on stepwise logistic regression and several classifiers with the leave-one-image-out method.

Input features	A_z value obtained by ROC analysis			FP/image at the specified sensitivity by FROC analysis					
				FLDA		Bayesian		ANN	
	FLDA	Bayesian	ANN	80%	90%	80%	90%	80%	90%
H_1	0.76	0.76	**0.77**	6.9	9.9	6.2	**8.7**	5.5	10.0
H_2	0.75	0.74	0.75	**5.4**	11.4	6.4	11.8	6.7	10.7
H_0	0.72	0.73	0.73	7.7	11.3	6.9	11.4	8.2	11.1

As illustrated in Table 2, with the leave-one-patient-out method, H_2 shows results comparable to those obtained with H_1. For both the feature sets, the highest A_z of 0.76 was obtained with FLDA. A sensitivity of 80% at 5.3 FP/image with the Bayesian classifier for H_1, and a sensitivity of 80% at 4.2 FP/image with FLDA for H_2 were obtained by FROC analysis and the leave-one-patient-out method.

The features based on H_1 and H_2, as proposed in the present work, have demonstrated improved performance as compared to H_0.[16] The results of FROC analysis are presented in Figures 5(a) and (b) for the leave-one-image-out and the leave-one-patient-out methods, respectively, using the FLDA classifier. Because the features used in the present study were computed from segmented breast images, the results obtained with H_0 are slightly different from those in a previous related paper.[16]

Table 2. Results of ROC and FROC analysis by using selected features based on stepwise logistic regression and several classifiers with the leave-one-patient-out method.

Input features	A_z value obtained by ROC analysis			FP/image at the specified sensitivity by FROC analysis					
				FLDA		Bayesian		ANN	
	FLDA	Bayesian	ANN	80%	90%	80%	90%	80%	90%
H_1	**0.76**	0.76	0.76	5.4	8.2	5.3	**7.4**	6.3	9.5
H_2	0.76	0.74	0.75	**4.2**	9.2	5.7	8.8	6.9	11.8
H_0	0.71	0.70	0.71	8.7	11.2	8.5	10.9	12.0	13.6

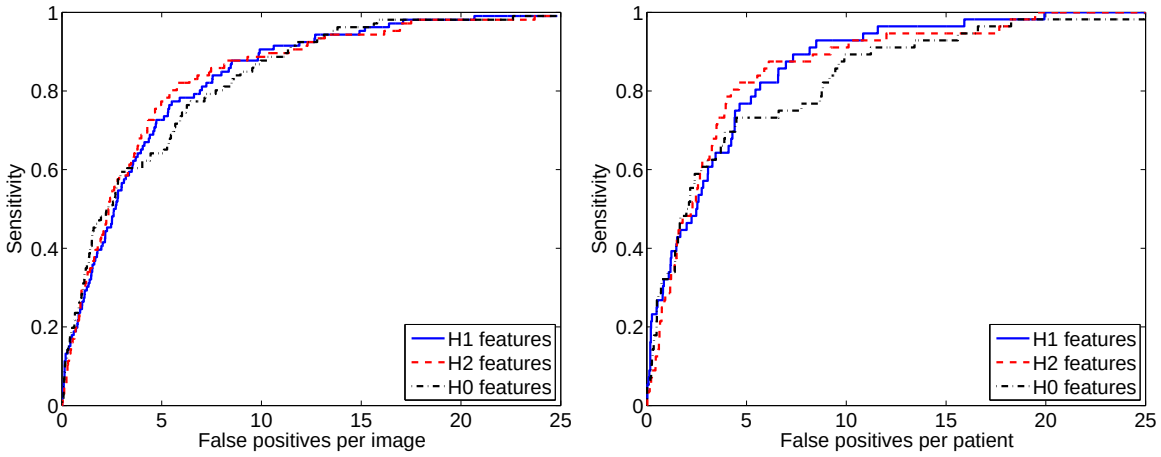

Figure 5. FROC curves obtained with (a) the FLDA classifier and the leave-one-image-out method, and (b) the FLDA classifier and the leave-one-patient-out method.

The feature sets were also compared in terms of the statistical significance of the differences between the ROC curves. Tables 3 and 4 illustrate the associated p-values obtained using ROCKIT[25] with the leave-one-image-out and the leave-one-patient-out methods, respectively. The results illustrate that the feature set H_1 provides ROC results that are better than those given by H_0 with high statistical significance (using the Bayesian or ANN classifier). The feature set H_2 has provided better results than H_0 with statistical significance in a few cases. Although H_1 has provided higher A_z values than H_2 in several cases, the difference is not statistically significant.

Table 3. Statistical significance, indicated by the p-value of the differences between the ROC curves, obtained for the three feature sets using three classifiers and the leave-one-image-out method. The p-values were estimated using ROCKIT (up to four decimal places).

	FLDA		Bayesian		ANN	
Feature set	H_2	H_0	H_2	H_0	H_2	H_0
H_1	0.3532	0.0174	0.0983	0.0009	0.1320	0.004
H_2		0.0327		0.0609		0.0980

Table 4. Statistical significance, indicated by the p-value of the differences between the ROC curves, obtained for the three feature sets using three classifiers and the leave-one-patient-out method. The p-values were estimated using ROCKIT (up to four decimal places).

	FLDA		Bayesian		ANN	
Feature set	H_2	H_0	H_2	H_0	H_2	H_0
H_1	1.0000	0.0137	0.1429	0.0005	0.3025	0.0042
H_2		0.0188		0.0350		0.0712

4. CONCLUSION

Statistical features derived from angle co-occurrence matrices, as proposed in the present work for the characterization of oriented patterns, have demonstrated improved performance as compared to similar features derived using GCMs for the purpose of detection of architectural distortion. Using fewer features, the sensitivity of 80% at 5.4 FP/image with the leave-one-image-out method, obtained in the present work, represents better results than those provided by previously developed methods.[16] Further work is in progress to combine the features proposed in the present work with previously developed features for improved and efficient detection of architectural distortion in prior mammograms of interval-cancer cases.

Acknowledgments: This project was funded by grants from the University International Grants Committee of the University of Calgary, the Shastri Indo-Canadian Institute, the Canadian Breast Cancer Foundation: Prairies/NWT Chapter, and the Natural Sciences and Engineering Research Council (NSERC) of Canada. Partially supported by Department of Information Technology, Government of India. During the period of research Jayasree Chakraborty has received institute scholarship from Indian Institute of Technology Kharagpur.

REFERENCES

[1] Knutzen, A. M. and Gisvold, J. J., "Likelihood of malignant disease for various categories of mammographically detected, nonpalpable breast lesions," *Mayo Clinic Proceedings* **68**, 454–460 (1993).

[2] American College of Radiology (ACR), *Illustrated Breast Imaging Reporting and Data System (BI-RADS)*, American College of Radiology, Reston, VA, fourth ed. (2003).

[3] Doi, K., "Computer-aided diagnosis in medical imaging: historical review, current status and future potential," *Computerized Medical Imaging and Graphics* **31**, 198–211 (2007).

[4] Tang, J., Rangayyan, R. M., Xu, J., Naqa, I. E., and Yang, Y., "Computer-aided detection and diagnosis of breast cancer with mammography: Recent advances," *IEEE Transactions on Information Technology in Biomedicine* **13**, 236–251 (March 2009).

[5] Baker, J. A., Rosen, E. L., Lo, J. Y., Gimenez, E. I., Walsh, R., and Soo, M. S., "Computer-aided detection (CAD) in screening mammography: Sensitivity of commercial CAD systems for detecting architectural distortion," *American Journal of Roentgenology* **181**, 1083–1088 (2003).

[6] Rangayyan, R. M., Ayres, F. J., and Desautels, J. E. L., "A review of computer-aided diagnosis of breast cancer: toward the detection of subtle signs," *Journal of the Franklin Institute* **344**, 312–348 (2006).

[7] Karssemeijer, N. and te Brake, G. M., "Detection of stellate distortions in mammograms," *IEEE Transactions on Medical Imaging* **15**, 611–619 (October 1996).

[8] Suckling, J., Parker, J., Dance, D. R., Astley, S., Hutt, I., Boggis, C. R. M., Ricketts, I., Stamakis, E., Cerneaz, N., Kok, S.-L., Taylor, P., Betal, D., and Savage, J., "The mammographic image analysis society digital mammogram database," in *Digital Mammography: Proceedings of the 2nd International Workshop on Digital Mammography*, Gale, A. G., Astley, S. M., Dance, D. D., and Cairns, A. Y., eds., 375–378, Elsevier, York, UK (July 1994).

[9] Ayres, F. J. and Rangayyan, R. M., "Reduction of false positives in the detection of architectural distortion in mammograms by using a geometrically constrained phase portrait model," *International Journal of Computer Assisted Radiology and Surgery* **1**, 361–369 (2007).

[10] Jasionowska, M., Przelaskowski, A., Rutczynska, A., and Wroblewska, A., "A two-step method for detection of architectural distortions in mammograms," in *Information Technologies in Biomedicine*, **69**, 73–84, Springer Berlin / Heidelberg (2010).

[11] Sumkin, J. H., Holbert, B. L., Herrmann, J. S., Hakim, C. A., Ganott, M. A., Poller, W. R., Shah, R., Hardesty, L. A., and Gur, D., "Optimal reference mammography: A comparison of mammograms obtained 1 and 2 years before the present examination," *American Journal of Roentgenology* **180**, 343–346 (2003).

[12] Varela, C., Karssemeijer, N., Hendriks, J. H. C. L., and Holland, R., "Use of prior mammograms in the classification of benign and malignant masses," *European Journal of Radiology* **56**, 248–255 (2005).

[13] Rangayyan, R. M., Prajna, S., Ayres, F. J., and Desautels, J. E. L., "Detection of architectural distortion in mammograms acquired prior to the detection of breast cancer using Gabor filters, phase portraits, fractal dimension, and texture analysis," *International Journal of Computer Assisted Radiology and Surgery* **2**, 347–361 (April 2008).

[14] Ciatto, S., Turco, M. R. D., and Zappa, M., "The detectability of breast cancer by screening mammography," *British Journal of Cancer* **71**(2), 337–339 (1995).

[15] Sameti, M., Ward, R. K., Morgan-Parkes, J., and Palcic, B., "Image feature extraction in the last screening mammograms prior to detection of breast cancer," *IEEE Journal of Selected Topics in Signal Processing* **3**, 46–52 (February 2009).

[16] Banik, S., Rangayyan, R. M., and Desautels, J. E. L., "Detection of architectural distortion in prior mammograms," *IEEE Transactions on Medical Imaging* **30**, 279–294 (February 2011).

[17] Rangayyan, R. M., Banik, S., and Desautels, J. E. L., "Computer-aided detection of architectural distortion in prior mammograms of interval cancer," *Journal of Digital Imaging* **23**, 611–631 (October 2010).

[18] Rangayyan, R. M., Banik, S., and Desautels, J. E. L., "Detection of architectural distortion in prior mammograms using measures of angular distribution," in *Proceedings of SPIE Medical Imaging 2011: Computer Aided Diagnosis*, Summers, R. M. and van Ginneken, B., eds., **796308-1-9** (February 2011).

[19] Alberta Cancer Board, www.cancerboard.ab.ca/screentest, Alberta, Canada, *Screen Test: Alberta Program for the Early Detection of Breast Cancer – 2001/03 Biennial Report* (2004).

[20] Alto, H., Rangayyan, R. M., and Desautels, J. E. L., "Content-based retrieval and analysis of mammographic masses," *Journal of Electronic Imaging* **14**(2), Article number 023016, 1–17 (2005).

[21] Haralick, R. M., "Statistical and structural approaches to texture," *Proceedings of the IEEE* **67**, 786–804 (May 1979).

[22] Haralick, R. M., Shanmugam, K., and Dinstein, I., "Textural features for image classification," *IEEE Transactions on Systems, Man, Cybernetics* **3(6)**, 610–622 (1973).

[23] Duda, R. O., Hart, P. E., and Stork, D. G., [*Pattern Classification*], Wiley-Interscience, New York, NY, 2nd ed. (2001).

[24] Haykin, S., [*Neural Networks: A Comprehensive Foundation*], Prentice Hall, NJ, second ed. (1999).

[25] "ROCKIT." Kurt Rossmann Laboratories for Radiologic Image Research. ROC Software. http://www-radiology.uchicago.edu/krl/roc_soft6.htm, accessed on February 20, 2010.